Coherent beam combining with an ultrafast multicore Yb-doped fiber amplifier

Patricia Ramirez, Marc Hanna, Géraud Bouwmans, Hicham El Hamzaoui, Mohamed Bouazaoui, Damien Labat, Karen Delplace, Julien Pouysegur, Florent Guichard, Philippe Rigaud, et al.

HAL Id: hal-01120367

https://hal-iogs.archives-ouvertes.fr/hal-01120367

Submitted on 19 Jun 2015

Coherent beam combining with an ultrafast multicore Yb-doped fiber amplifier

Lourdes Patricia Ramirez,[1] Marc Hanna,[1,*] Géraud Bouwmans,[2] Hicham El Hamzaoui,[2] Mohamed Bouazaoui,[2] Damien Labat,[2] Karen Delplace,[2] Julien Pouysegur,[1,3] Florent Guichard,[1,3] Philippe Rigaud,[4] Vincent Kermène,[4] Agnès Desfarges-Berthelemot,[4] Alain Barthélémy,[4] Florian Prévost,[5] Laurent Lombard,[5] Yoann Zaouter,[3] Frédéric Druon,[1] and Patrick Georges[1]

[1]*Laboratoire Charles Fabry, Institut d'Optique, CNRS, Université Paris-Sud, 2 Avenue Augustin Fresnel, 91127 Palaiseau, France*
[2]*Laboratoire PhLAM UMR 8523, Institut IRCICA USR CNRS 3380, Université Lille 1, 50 Avenue Halley, 59658 Villeneuve d'Ascq Cedex, France*
[3]*Amplitude Systèmes, 11 avenue de Canteranne, Cité de la Photonique, 33600 Pessac, France*
[4]*XLIM Institut de Recherche,UMR 7252, Université de Limoges CNRS, 123 Avenue Albert Thomas, 87060 Limoges, France*
[5]*Office National d'Etudes et de Recherches Aérospatiales, Département d'Optique Théoriques et Appliquée, Chemin de la Hunière, 91761 Palaiseau, France*
[*]*marc.hanna@institutoptique.fr*

Abstract: Active coherent beam combination using a 7-non-coupled core, polarization maintaining, air-clad, Yb-doped fiber is demonstrated as a monolithic and compact power-scaling concept for ultrafast fiber lasers. A microlens array matched to the multicore fiber and an active phase controller composed of a spatial light modulator applying a stochastic parallel gradient descent algorithm are utilized to perform coherent combining in the tiled aperture geometry. The mitigation of nonlinear effects at a pulse energy of 8.9 µJ and duration of 860 fs is experimentally verified at a repetition rate of 100 kHz. The experimental combining efficiency results in a far field central lobe carrying 49% of the total power, compared to an ideal value of 76%. This efficiency is primarily limited by group delay differences between cores which is identified as the main drawback of the system. Minimizing these group delay issues, e.g. by using short and straight rod-type multicore fibers, should allow a practical power scaling solution for femtosecond fiber systems.

OCIS codes: (060.2320) Fiber optics amplifiers and oscillators; (140.3298) Laser beam combining; (140.7090) Ultrafast lasers; (060.4005) Microstructured fibers.

References and links

1. J. Limpert, O. Schmidt, J. Rothhardt, F. Röser, T. Schreiber, A. Tünnermann, S. Ermeneux, P. Yvernault, and F. Salin, "Extended single-mode photonic crystal fiber lasers," Opt. Express **14**(7), 2715–2720 (2006).
2. T. Eidam, J. Rothhardt, F. Stutzki, F. Jansen, S. Hädrich, H. Carstens, C. Jauregui, J. Limpert, and A. Tünnermann, "Fiber chirped-pulse amplification system emitting 3.8 GW peak power," Opt. Express **19**(1), 255–260 (2011).
3. F. Stutzki, F. Jansen, H.-J. Otto, C. Jauregui, J. Limpert, and A. Tünnermann, "Designing advanced very-large-mode-area fibers for power scaling of fiber-laser systems," Optica **1**(4), 233–242 (2014).
4. E. Seise, A. Klenke, S. Breitkopf, M. Plötner, J. Limpert, and A. Tünnermann, "Coherently combined fiber laser system delivering 120 µJ femtosecond pulses," Opt. Lett. **36**(4), 439–441 (2011).
5. L. Daniault, M. Hanna, L. Lombard, Y. Zaouter, E. Mottay, D. Goular, P. Bourdon, F. Druon, and P. Georges, "Coherent beam combining of two femtosecond fiber chirped-pulse amplifiers," Opt. Lett. **36**(5), 621–623 (2011).
6. Y. Zaouter, L. Daniault, M. Hanna, D. N. Papadopoulos, F. Morin, C. Hönninger, F. Druon, E. Mottay, and P. Georges, "Passive coherent combination of two ultrafast rod type fiber chirped pulse amplifiers," Opt. Lett. **37**(9), 1460–1462 (2012).

7. A. Klenke, E. Seise, S. Demmler, J. Rothhardt, S. Breitkopf, J. Limpert, and A. Tünnermann, "Coherently-combined two channel femtosecond fiber CPA system producing 3 mJ pulse energy," Opt. Express **19**(24), 24280–24285 (2011).
8. L. Michaille, C. R. Bennett, D. M. Taylor, T. J. Shepherd, J. Broeng, H. R. Simonsen, and A. Petersson, "Phase locking and supermode selection in multicore photonic crystal fiber lasers with a large doped area," Opt. Lett. **30**(13), 1668–1670 (2005).
9. X.-H. Fang, M.-L. Hu, B.-W. Liu, L. Chai, C.-Y. Wang, and A. M. Zheltikov, "Generation of 150 MW, 110 fs pulses by phase-locked amplification in multicore photonic crystal fiber," Opt. Lett. **35**(14), 2326–2328 (2010).
10. M. Paurisse, M. Hanna, F. Druon, and P. Georges, "Wavefront control of a multicore ytterbium-doped pulse fiber amplifier by digital holography," Opt. Lett. **35**(9), 1428–1430 (2010).
11. I. Hartl, A. Marcinkevičius, H. A. McKay, L. Dong, and M. E. Fermann, "Coherent Beam Combination Using Multi-Core Leakage-Channel Fibers," in *Advanced Solid-State Photonics*, OSA Technical Digest Series (CD) (Optical Society of America, 2009), paper TuA6.
12. Ph. Rigaud, V. Kermene, G. Bouwmans, L. Bigot, A. Desfarges-Berthelemot, D. Labat, A. Le Rouge, T. Mansuryan, and A. Barthélémy, "Spatially dispersive amplification in a 12-core fiber and femtosecond pulse synthesis by coherent spectral combining," Opt. Express **21**(11), 13555–13563 (2013).
13. H. El Hamzaoui, L. Bigot, G. Bouwmans, I. Razdobreev, M. Bouazaoui, and B. Capoen, "From molecular precursors in solution to microstructured optical fiber: a Sol-gel polymeric route," Opt. Mater. Express **1**, 234–242 (2011).
14. A. Baz, H. El Hamzaoui, I. Fsaifes, G. Bouwmans, M. Bouazaoui, and L. Bigot, "A pure silica ytterbium-doped sol–gel-based fiber laser," Laser Phys. Lett. **10**(5), 055106 (2013).
15. M. A. Vorontsov and V. P. Sivokon, "Stochastic parallel-gradient-descent technique for high-resolution wave-front phase-distortion correction," J. Opt. Soc. Am. A **15**(10), 2745–2758 (1998).
16. L. Liu and M. A. Vorontsov, "Phase-Locking ot Tiled Fiber Array using SPGD Feedback Controller," Proc. SPIE **5895**, 58950P (2005).
17. S. M. Redmond, K. J. Creedon, J. E. Kansky, S. J. Augst, L. J. Missaggia, M. K. Connors, R. K. Huang, B. Chann, T. Y. Fan, G. W. Turner, and A. Sanchez-Rubio, "Active coherent beam combining of diode lasers," Opt. Lett. **36**(6), 999–1001 (2011).
18. F. Guichard, M. Hanna, L. Lombard, Y. Zaouter, C. Hönninger, F. Morin, F. Druon, E. Mottay, and P. Georges, "Two-channel pulse synthesis to overcome gain narrowing in femtosecond fiber amplifiers," Opt. Lett. **38**(24), 5430–5433 (2013).
19. M. Hanna, D. N. Papadopoulos, L. Daniault, F. Druon, P. Georges, and Y. Zaouter, "Coherent beam combining in the femtosecond regime," Chapter 9 in "Coherent laser beam combining", Ed. Arnaud Brignon, Wiley-VCH, ISBN 978–3–527–41150–4, pp 277–301 (2013).
20. J. Bourderionnet, C. Bellanger, J. Primot, and A. Brignon, "Collective coherent phase combining of 64 fibers," Opt. Express **19**(18), 17053–17058 (2011).
21. J. Lhermite, E. Suran, V. Kermene, F. Louradour, A. Desfarges-Berthelemot, and A. Barthélémy, "Coherent combining of 49 laser beams from a multiple core optical fiber by a spatial light modulator," Opt. Express **18**(5), 4783–4789 (2010).
22. H.-J. Otto, A. Klenke, C. Jauregui, F. Stutzki, J. Limpert, and A. Tünnermann, "Scaling the mode instability threshold with multicore fibers," Opt. Lett. **39**(9), 2680–2683 (2014).

1. Introduction

Performance scaling of fiber lasers, especially ultrafast fiber lasers, has attracted much interest in the past few years driven by the demand for high energy, high peak power and high repetition rate sources. Progress in developing high power ultrafast fiber lasers has mainly been limited by nonlinear effects caused by high intensities confined within the small core of the fiber, eventually leading to pulse distortion and material damage. The first approach for mitigating nonlinearities evidently relies on fabricating fibers with larger effective areas [1]. Up to date, the highest peak power delivered from an ultrafast fiber laser system (3.8 GW, 2.2 mJ) exploited a single-core, very large mode area fiber with a mode field diameter around 18 times larger than a standard step index fiber [2]. The constraint though in this strategy is the difficulty to preserve single-mode operation, requiring intricate and rigorous analysis for realizing optimum fiber designs [3]. The second approach is coherent beam combination (CBC) which involves the amplification of a seed beam in separate channels and coherent or in-phase combination at the output. CBC of two femtosecond fiber amplifiers was first demonstrated to retain the temporal and spectral characteristics of each channel with a combining efficiency of 90% [4,5]. As all amplifiers must be in phase, CBC architectures must eliminate any phase differences via passive or active phase locking methods. Both have proven to be successful with output peak powers and energies reaching 2 GW/0.65 mJ for

passive schemes [6] and 5.4 GW/3 mJ for active schemes [7], already surpassing the record of a single large mode area amplifier. Coherent beam combination of large mode area fibers is a promising method to drastically improve the power capabilities of fiber-based systems but much effort for adapting these architectures for N-amplifiers is still needed. Utilizing separate amplifiers necessitates individual pumps and individual phase modulators for active phase-locking. An alternative solution based on the use of a multicore fiber (MCF) may offer advantages allowing common pump and phase modulators and more compact amplification schemes.

A multicore fiber is essentially an integrated version of CBC and large mode area fibers. The fiber effective area increases with the number of cores and each core has to be phase locked for efficient combination. Coupled-core MCFs have been proven to deliver high energy, nanosecond pulses (2.2 mJ) [8] and moderate peak power, femtosecond pulses (150 MW) [9] wherein the individual cores were phase-locked via supermode selection. However, this passive technique was pump-power dependent, making power-scaling a challenging task. An active phase-locking technique based on digital holography [10] provided results independent of the pump power in the nanosecond regime. This technique though posed difficulties for direct application in the femtosecond regime since wavefront measurement was necessary in the setup. On the other hand, independent-core MCFs are also attractive for power-scaling as shown in [11]. Non-coupled cores act as individual waveguides whose phases are individually addressable as in active CBC for separate amplifiers. Furthermore, contained within a single fiber, all cores are then coupled in terms of mechanical and thermal conditions which decreases the phase differences between channels. A collective pump for all cores and a common phase modulator seems feasible with this architecture. Recently, a 12-core MCF was employed for amplification and coherent spectral synthesis of femtosecond pulses only using a deformable mirror to adjust the phase of the individual cores [12]. It was shown that an active controller was not necessary once phase differences were matched.

In this work, the applicability and limitations of an independent-core, ytterbium-doped multicore fiber for ultrafast pulse amplification and active coherent beam combination are investigated for the first time. This innovative power-scaling architecture proposes a monolithic and compact setup as compared to combining individual amplifiers. A microstructure, 7-core, Yb-doped fiber was designed and fabricated for the experiments and is presented in the next section. The amplifier uses a single pump and a common phase modulator to individually address the phases of each core. The phase noise between cores was measured then a simple active phase controller based on a spatial light modulator (SLM) implementing a stochastic parallel gradient descent (SPGD) algorithm was installed. Active coherent beam combining is achieved in the tiled aperture geometry using a microlens array matched to the multicore fiber. This proof of principle experiment shows the viability of independent-core MCFs for performance scaling in fiber lasers.

2. Double clad Yb-doped multicore fiber

An image of the MCF used in this work is shown in Fig. 1. The fiber was fabricated by IRCICA via stack and draw technology. It consists of seven Yb-doped cores, prepared using the sol-gel technique [13,14], arranged in a hexagonal pattern with an inner cladding designed for high-power diode pumping. All cores are single mode at the seed wavelength of 1030 nm and have a mode field diameter of 16 μm. The effective area of a single core is 200 μm^2, resulting to a total effective area of 1400 μm^2. Air holes in the periodic structure have a diameter of 4.4 μm. Additionally, the MCF is polarization maintaining, owing to the boron rods placed adjacent to the cores which introduce a birefringence of 5 x 10^{-5}. The index contrast between Yb-doped cores and silica is estimated to 0.0004, while that of boron rods and silica is about −0.009. Separated by a pitch of 45 μm, coupling between cores is negligible and each acts as an isolated waveguide. This was verified by selective injection of one core: after 1 m of propagation in the multicore fiber, the ratio of power in the excited core

and the neighboring cores is higher than 20 dB. An air clad within the fiber forms a second guiding structure for the pump. This inner cladding has a diameter of around 190 μm and NA of 0.43. For a fiber length of 4.5 m, pump absorption at 976 nm is measured to be 20 dB.

Group delay differences between cores in such a fiber can arise from variable physical path differences between cores induced by bending/twisting the fiber and from inhomogeneities in the effective indices of each core which are inherent upon fabrication. The effective index of each core is influenced by variations in the index profile that depend on both the size and the refractive index of the doped cores. To decouple these origins, the group delay was measured for each core using a spectral interferometry setup. A 65 cm-long piece of the MCF was maintained straight and characterized, yielding a group-velocity difference standard deviation of 100 fs/m. This value corresponds to a variation of the group delay and equivalently, a refractive index variation of only 0.002%. Despite being minute, the group-velocity difference is non-negligible in our case as a few meters of amplifying fiber are used to amplify 500 fs pulses.
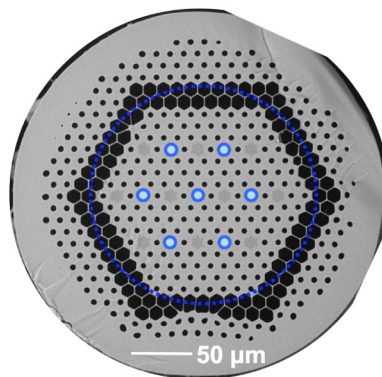

Fig. 1. Image of the double-clad Yb-doped multicore fiber. The seven cores of the fiber are highlighted with blue circles while the dark blue circle indicates the inner cladding. Boron rods (dark gray zones) placed adjacent to each core makes the MCF polarization maintaining.

3. Experimental setup

The MCF is implemented in a chirped pulse amplification configuration with counter-propagating seed and pump beams as depicted in Fig. 2(a). An all-fiber front end consisting of a passively mode-locked oscillator, a pulse picker, a fiber stretcher and a pre-amplifier provides the stretched seed of 500 ps for injection. Controlling the acousto-optic modulator pulse picker permits easy variation of the repetition rate from 100 kHz to 40 MHz and seed energy from 520 to 4 nJ. The spectrum of the front end, centered at 1030 nm, has a FWHM of 7 nm and is compressible down to 585 fs (autocorrelation FWHM). Seeding the individual cores of the MCF is carried out with a computer-controlled SLM. The SLM displays a phase map equivalent to the sum of seven maps, each of which represents a grating that diffracts the beam to one core. The seed beam is focused at the input facet of the MCF and seven beams form at the focal spot, matching the location and mode field diameter of the cores. The coupling efficiency of the seed beam is estimated to be 49% due to the diffraction efficiency of the SLM. As illustrated in Fig. 2(a), an optical isolator is inserted between the amplifier and SLM to prevent any unabsorbed pump from damaging it (damage threshold = 2 W/cm^2). The 4.5-m MCF is carefully arranged to ensure the lowest group delay between all cores by incorporating a specific combination of loops/twists in the fiber geometric configuration. This optimum fiber arrangement is tested experimentally and is identified by maximizing the fringe visibility at the far field output of the fiber. Fringe visibility is directly related to the coherence between cores and their group delay differences as discussed in section 5.1. To combine the multibeam output, a microlens array (MLA, f$_{MLA}$ = 0.4 mm, pitch = 45 μm, lens

diameter = 34 μm) at the output facet collimates the individual beams from each core. Afterwards, a dichroic mirror reflects the multibeam output for phase noise characterization as shown in Fig. 2(b) or for coherent beam combination and pulse compression as illustrated in Fig. 2(c). The pump of the amplifier, a 20-W fiber-coupled laser diode at 976 nm, is focused into the inner cladding of the MCF. The presence of the MLA in the pump beam path does not make coupling problematic although a minor decrease in the pump coupling efficiency is observed.

Using a SLM for injecting the beam into the MCF offers two advantages: (1) the capability to selectively excite cores and (2) independent phase control of each core by a simple translation of the diffracting fringe pattern. To measure the phase noise of the amplifier, the seed beam is coupled into two adjacent cores. The MLA is removed, permitting interference between both beams and the formation of vertical fringes at the far field (see Fig. 2(b)). These fringes are exploited to have in-phase and quadrature signals. A first photodiode (PD1) is initially positioned at the maximum of a bright fringe (in-phase output) while a second (PD2) is fixed at the median value (quadrature output). The phase noise is then easily extracted via the relation $\phi(t) = \tan^{-1}\left(V_{PD2}/V_{PD1}\right)$ where V_{PD1} and V_{PD2} are the normalized signals from the photodiodes. Knowledge about the amplifier phase noise demonstrates the benefits of using a MCF over separate fiber amplifiers as discussed in the next section. The phase noise characteristics are also valuable to determine the bandwidth requirement and best approach for feedback control to coherently combine the output of the MCF.
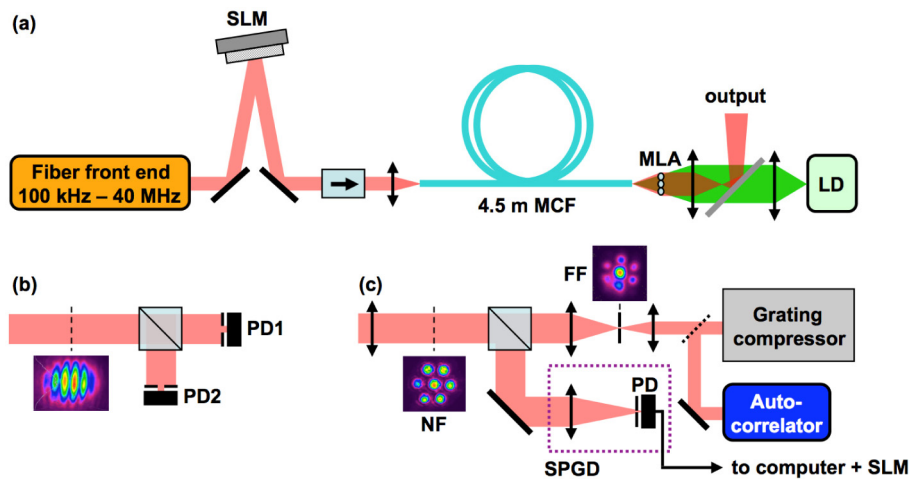

Fig. 2. Experimental setup of the MCF amplifier. (a) Coupling of the seed and pump beams into the fiber. The seed beam is shaped with a spatial light modulator (SLM) for injection in the 7-core MCF and is collimated by a microlens array (MLA). The pump laser diode (LD) is coupled at the output end of the fiber. (b) Phase noise characterization setup with a quadrature detector composed of a beamsplitter and two photodiodes (PD). (c) Phase locking of the output via a stochastic parallel gradient descent (SPGD) feedback loop and compression of the combined beam. Near field (NF) and far field (FF) images of the beam are included.

The complete setup for coherent beam combination and pulse compression includes Fig. 2(c) at the output of the MCF amplifier. The near field (NF) output of the amplifier is formed by the seven separate cores collimated by the microlens array. Afterwards, the beam is divided in two where one part is used for feedback control while the other for pulse compression and temporal/spectral characterization. The phases of all cores are locked by implementing a stochastic parallel gradient descent [15] optimization loop which is a simple yet powerful method for active phasing in coherent beam combination systems [16,17]. SPGD is an optimization algorithm where small random perturbations are introduced into a system, their effect on a cost function is measured and then this information is used to calculate the

correction necessary to maximize or minimize the cost function. In the setup, random phase perturbations are simultaneously introduced to the seven cores with the SLM, the cost function is the intensity of the central lobe in the far field and a computer calculates the correction phases that are loaded onto the SLM. The bandwidth of the system is determined to be around 2 Hz. The low bandwidth is limited by the time required to calculate and display phase on the SLM and to measure the corresponding change in the cost function. The cost function is measured with a pinhole in front of a photodiode at the focal plane of a focusing lens. Once the cores are phase locked such that the cost function is maximized, the far field (FF) beam as shown in Fig. 2(c) is filtered to select the central lobe. This central lobe is then compressed with a grating compressor (1750 l/mm) and its pulse duration is measured with an autocorrelator.

4. Phase noise characterization of MCF and comparison with separate fiber amplifiers

The time series of the phase noise between two adjacent cores in the MCF (blue) and two separate double-clad (DC) fiber amplifiers (green) is shown in Fig. 3(a) for a total duration of 50 s. The phase noise for the DC amplifiers was measured from the setup presented in [18] at a comparable output power as the MCF of 1.5 W. Each DC amplifier was 2-m in length. The graph shows a significantly larger amount of phase noise for two separate fiber amplifiers with a total peak-peak difference in phase of 180 rad as compared only 2.6 rad for two cores in an MCF. The maximum phase difference in the MCF is almost 70 times less than the separate fiber amplifiers. This result highlights the most significant advantage of using a MCF for coherent beam combining: due to their proximity, cores in the MCF are coupled thermally and mechanically, reducing the phase fluctuations between the cores. Moreover, with the smaller and slower phase difference, the requirements of the feedback control system to phase lock all cores become less demanding.
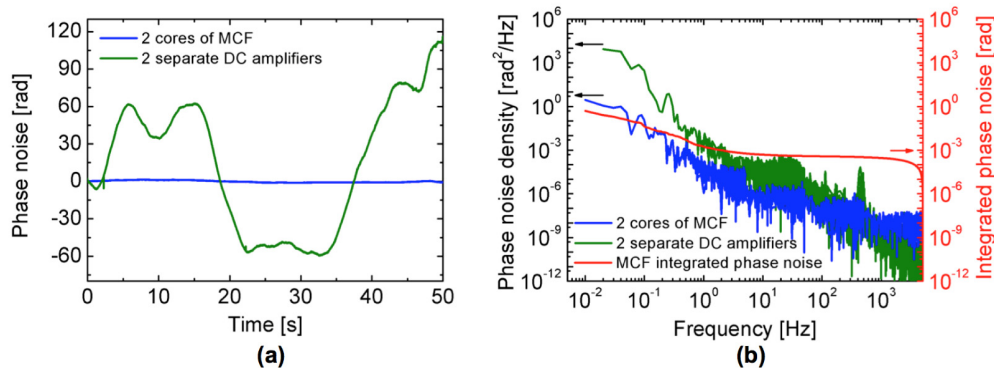

Fig. 3. Comparison between the (a) phase noise and (b) phase noise density between two cores of the MCF (blue) and two separate DC fiber amplifiers (green). The integrated phase noise of the MCF is shown in red.

The phase noise spectral density comparison of both cases is shown in Fig. 3(b). In general, low frequencies (<1 Hz) contribute to a substantial amount to the phase noise. The phase noise density in the MCF is well below the separate amplifiers case, especially at low frequencies up to around 1 Hz where it is 3 orders of magnitude lower. The integrated phase noise for the MCF is included as well in Fig. 3(b) to emphasize that low frequency components below 1 Hz constitute the most significant part of overall phase fluctuations. Consequently, to stabilize the phase of the cores a controller bandwidth of a few Hz will be sufficient and the available SPGD controller with a bandwidth of 2 Hz is applicable for the system.

5. Coherent beam combination with the multicore fiber amplifier

5.1. Phase locking

One of the main characteristics of the tiled aperture coherent combining geometry compared to the filled aperture is that the spatial profile of the output beam is correlated to the quality of coherent combining. The combined beam shape at the output of the multicore fiber amplifier is extremely sensitive to the phase difference between its cores. The active phase controller which employs an SLM for phase adjustment, is thus essential in the setup for two reasons: its main task is to find the optimum phase for all cores to achieve the best beam combination while its secondary task is to maintain this phase relationship in the presence of phase noise/phase drifts in the system. Furthermore, in the femtosecond regime, and even in the case of perfect phase locking, group delay differences among cores induce a decrease in the visibility of the spatial features due to coherent addition. These group delay differences cannot be corrected with the SLM since it only allows phase adjustment up to 2π. In the extreme case where the group delay differences are larger than the pulsewidth, the output beam corresponds to the incoherent addition of the individual cores and coherent effects are washed out. This feature is used experimentally to optimize the fiber geometric configuration and minimize group delay differences. Moreover, such group delay differences also introduce spatio-temporal couplings in the output beam [19].
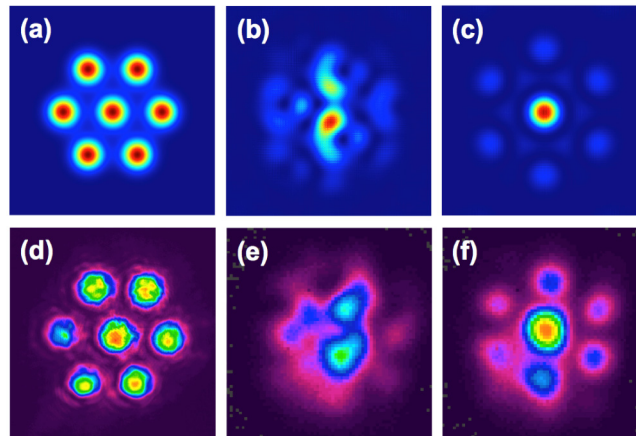

Fig. 4. Comparison between (a-c) simulated and (d-f) experimental near field and far field beams of the MCF. (a,d) Near field image consisting of cores collimated by a microlens array, (b,e) far field images when the cores have random phases or are not phase locked via SPGD, (c,f) far field images when the cores have locked phases or after phase locking via SPGD.

Prior to performing the experiment and installing the SPGD active controller, simulations are performed to (1) visualize the spatial profile of the combined beam, (2) understand spatial effects of phase differences between cores and (3) determine the best achievable combining efficiency from the setup. The simulation consists in getting the Fourier transform of the near field beam corresponding to the seven cores collimated by a MLA. The collimated beam is comprised of a central core surrounded by six other beams arranged in a hexagon with a pitch of 45 μm. The beam diameters, together with their individual amplitude and phase, are modifiable in the program to model collimation adjustment and to introduce random phases in each core. Figure 4(a) shows the collimated beams with diameters of 34 μm, matching the specifications of the microlens array. Figure 4(b) is the far field image of the beam or simply the Fourier transform of Fig. 4(a) with the cores having random phases while Fig. 4(c) is the ideal case with all cores having the same phase. Figure 4(b) shows the sensitivity of the output beam to the phases between the cores. A central spot cannot be identified in this case and the

combining efficiency is difficult to define. On the other hand, Fig. 4(c) corresponds to the target spatial profile at the output of the MCF amplifier where all cores have the same phase values. The central spot denotes the useable part of the beam in most applications, while the surrounding lobes are related to the non-perfect filling factor. The combining efficiency can accordingly be defined as the energy contained in the central spot over the total energy of the beam, meaning including the surrounding lobes. In our case, the theoretical combining efficiency in Fig. 4(c) is calculated to be 76% because of the non-perfect filling factor of the near field which is due to the difference of the lens diameter of 34 μm from the fiber pitch of 45 μm. Higher combining efficiencies are thus attainable if the diameter of the microlenses approaches the pitch of the fiber and the mode size of each beam matches this diameter (e.g. ~90% is achievable for a mode and lens diameter of 40.5 μm). The lens size, however, is a technical limitation in the fabrication of the microlens array. Techniques such as flat beam shaping can be used to improve the combining efficiency in this tiling approach.

The experimental near field and far field images of the MCF when pumped with a power of 7 W and seeded with 63 mW at 10 MHz are shown in Figs. 4(d-f). Similar images are obtained at higher pump powers. Figure 4(d) is the near field output of the MCF that is acquired by imaging the MLA onto a camera. With an understanding of the effects of random and locked phases on the far field beam, the SPGD active controller is installed and tested. A typical far field beam without locking the phases of all cores is shown in Fig. 4(e). The phase sensitivity of the setup is also confirmed as merely touching the fiber causes changes in the far field beam. Turning on the feedback controller leads to the maximization of the signal on the SPGD photodiode (see Fig. 2(c)) and after around 30 s, the far field beam converges to Fig. 4(f), similar to the theoretical far field beam. The experimental combining efficiency is measured to be 49%, lower than the theoretical value of 76%, as observed in other setups of coherent combining in tiled aperture configuration [20]. The deviation can be caused by residual phase differences, group delay differences between cores and intensity variations among the beams as observed in Fig. 4(d). This discrepancy in the amplification of each core is most likely an outcome of non-uniform pump absorption. As shown in Fig. 2, the cores are embedded within an air clad which is not perfectly symmetric and localized defects in the air clad itself may cause variations of pump absorption over the length of the fiber. In [21], a lower combining efficiency for a 49-core MCF seeded with femtosecond pulses was also observed for a short (0.6 m) and straight fiber, emphasizing the effect of core inhomogeneities on the group delay. In addition, a slight decrease in the combining efficiency to 45% is obtained at the highest pump power of 17.5 W (see inset Fig. 5(a)). Contrast degradation is observed in the spatial profile of the combined beam indicating that the decrease in combination efficiency could be caused by the larger discrepancies in intensity between cores at higher powers or the presence of nonlinear phase.

5.2. Temporal and spectral characterization

With access to the combined beam, temporal characterization is performed with an autocorrelator. Note that all pulse durations here and in the succeeding section are reported with the autocorrelation FWHM. Figure 5(a) presents a comparison between the autocorrelation of 1 core and 7 cores. Measurements are obtained at a repetition rate and seed power of 10 MHz/63 mW (6.3 nJ) and maximum pump power at 17.5 W. The output powers of the amplifier measured at the near field are 0.97 and 2.6 W respectively. The low energy level allows us to investigate linear effects such as the impact of differential group delays on the combined pulse duration. The differential group delays coming from the combination of 7 cores do not have a strong effect on the duration and shape of the pulse as seen in Fig. 5(a). Both pulses exhibit the same shape and have similar pulse durations: 640 fs for the single core (blue) and a slightly longer duration of 690 fs for the combined beam (green). Inset in the graph is the far field image of the combined beam showing the previously mentioned contrast

degradation at high pump powers. M^2 measurements of the central lobe yield 1.4 and 1.8 for the x and y axes respectively.

The spectrum of the combined beam (green) is shown in Fig. 5(b) together with the spectrum of a single core (blue) and the input seed (black). The FWHM spectral bandwidths for all three cases are similar (~7 nm) and the 7-core spectrum is narrower than the input spectrum by only 1 nm, confirming that most of the spectral content is contained within the far field central lobe. It is worth mentioning that the 7-core spectrum is an average over the entire central lobe of the combined beam. However, when the spectral contents of different regions of the beam are inspected, spatial inhomogeneity is observed in both the vertical and horizontal directions. As shown in Figs. 5(c) and (d), the left and bottom parts of the beam (red) have spectra which appear to be redshifted as compared to the center (green); the opposite occurs for the right and top parts (blue) with spectra that are blueshifted. The noticeable spatial inhomogeneity is a direct consequence of the differential group delay between cores as explained in [19]. Indeed, this is eliminated for single core excitation and when a short (1.4 m), straight fiber is used for coherent combination. Furthermore, with this spatio-temporal coupling in the combined beam, the differential group delay can therefore be related to the spatial beam quality, which may explain the non-ideal M^2 values of the central lobe stated earlier.
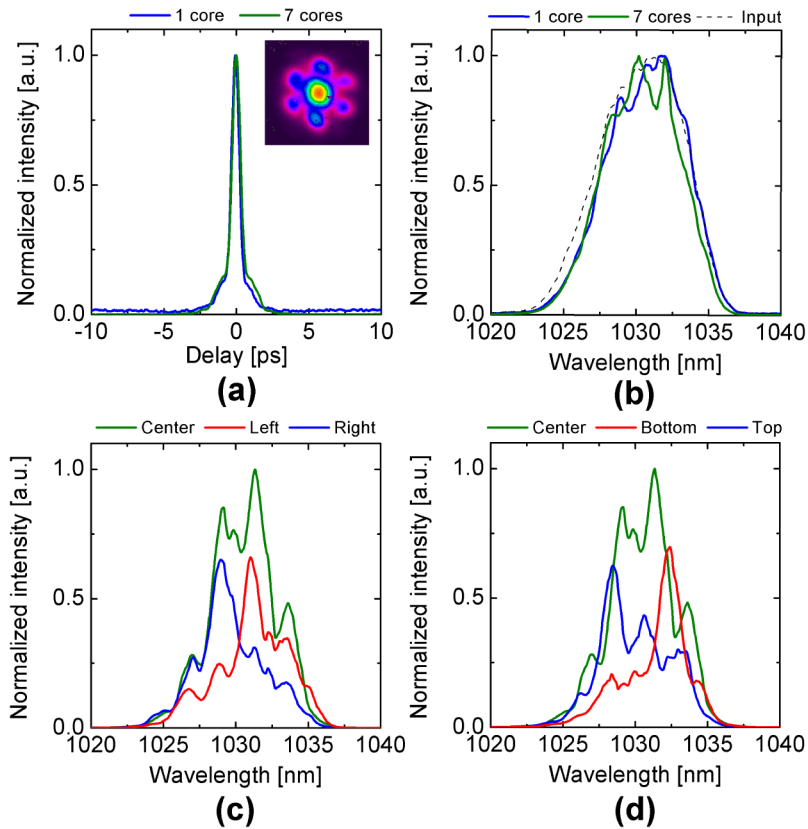

Fig. 5. (a) Autocorrelation of the compressed pulses and (b) spectra when 1 core (blue) and all 7 cores (green) are excited in the fiber with a seed repetition rate of 10 MHz, power of 63 mW and maximum pump power of 17.5 W. Inset in (a) is the far field spatial profile of the combined beam. The spectrum of the input seed beam is also indicated in (b). Spectra across the central lobe in the (c) horizontal and (d) vertical directions.

5.3. Mitigation of nonlinearities

Lastly, the amplifier is operated in the nonlinear regime by decreasing the repetition rate to 100 kHz, leading to an input seed power of 25 mW and higher seed energy of 0.25 µJ. Figure 6 is obtained with a constant output power of 890 mW (8.9 µJ) by adjusting the pump power for the single (blue) and 7-core excitation (green) cases. The autocorrelations clearly demonstrate the benefits of using the MCF for decreasing the detrimental effects of nonlinear phase in the amplifier. When all the power of the seed is injected into one core and pumped with the maximum available power, the quality of the compressed pulse degrades as evidenced in Fig. 6. The pulse shape is distorted with the presence of sidelobes, a long pedestal and a pulse duration of 920 fs. In this case, the estimated nonlinear phase is 22.7 rad. By dividing the seed into 7 channels, the nonlinear phase in each channel is thus one-seventh of that of a single core (3.2 rad). The quality of compressed pulse is good and has a duration of 860 fs. The slight lengthening of the pulse is mostly caused by the nonlinear phase and partially due to the group delay differences between the cores as observed in Fig. 5(a). This promising result confirms the capabilities of the MCF in providing larger effective areas for ultrashort pulse amplification via CBC of separate cores.

Energies up to 20 µJ are accessible with this MCF amplifier but with the large amount of nonlinear phase in the system, phase-locking between cores becomes difficult once the output energy exceeds 10 µJ. The SPGD optimization loop introduces random phase perturbations in each core and causes intensity fluctuations which in turn, directly affects the nonlinear phase. Consequently, when there are a lot of nonlinearities in the system, the phase-locking loop itself will add more phase noise, making convergence to best combined beam (Fig. 4(f)) problematic.
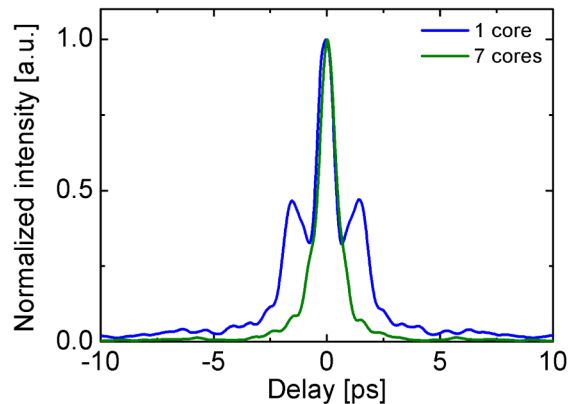

Fig. 6. Autocorrelation of the compressed pulses for an excitation of 1 core (blue) and all 7 cores (green) at a repetition rate of 100 kHz. The pump power of the amplifier is selected to maintain a constant output power of 0.89 W whether 1 or 7 cores are excited.

6. Conclusion

A new approach for power-scaling ultrafast lasers based on a Yb-doped multicore fiber amplifier is demonstrated for the first time. Interest in this architecture arises as a multicore fiber has the potential of offering a larger effective area than state of the art LMA fibers by spreading the total effective area over a number of smaller cores which easily maintain single-mode operation. In addition, due to the double-clad design of the MCF, pumping of seven cores is achieved with a single pump. This monolithic solution only requires one phase modulator and a less demanding feedback control system for coherent beam combination since its individual cores are under the same environmental conditions. Moreover, distributing the amplification of the seed pulse between seven cores is verified to reduce the nonlinearities in the amplifier as compared to using a single core.

Differential group delays between cores are identified as the essential limitation of the architecture, generally causing lower combining efficiencies and spectral inhomogeneity in the combined beam. Minimization of these group delay differences is a necessity to enhance the performance of the MCF amplifier. The fabrication process of the fiber might be improved to decrease inter-core inhomogeneity by precisely controlling the core sizes and refractive indices. Use of a segmented mirror would permit fine control of the group delay in each core, allowing a further reduction of these differential delays. Finally, a more straightforward solution would be to use short and straight fibers with low inter-core inhomogeneities—encouraging the development of rod-type, large mode area, multicore fibers [22].

Acknowledgments